

Lateral Water Diffusion in an Artificial Macroporous System: Modeling and Experimental Evidence

P. Castiglione,* B. P. Mohanty, P. J. Shouse, J. Simunek, M. Th. van Genuchten, and A. Santini

ABSTRACT

In two-domain schematizations of macroporous soils or fractured rock systems, lateral mass exchange between macropores and the soil matrix is generally modeled as an apparent first-order process. With respect to lateral diffusion, the system is thus characterized by a single parameter, the transfer rate coefficient, which is difficult to estimate a priori. We conducted water infiltration experiments in a laboratory column with an artificial macropore. The novel design of the experimental setup allowed us to discriminate between matrix flow and macropore flow, from which we could estimate the water exchange flux between the two domains. Most of the parameters in a dual-permeability model could be determined independently of the experimental data. In particular, a theoretical expression for the transfer rate coefficient was derived by assuming lateral water and solute diffusion to be similar processes. Numerical analysis of the water exchange process revealed that the transfer coefficient depended also on the macropore conductivity. When this dependency was taken into account, the model reproduced the experimental data reasonably well.

MOST DETERMINISTIC APPROACHES for modeling preferential flow in macroporous soils or unsaturated fractured rock rely on two- or multidomain continuum assumptions (Smettem and Kirkby, 1990; Cushman, 1990; Othmer et al., 1991; Pruess, 1999; National Resource Council, 2001). Typically, heterogeneous media are modeled as two overlapping porous systems, a high permeability domain associated with the macropore or fracture network and a low permeability domain associated with the matrix blocks. Exchange of mass (water and/or solute) between the two systems will occur in response to nonequilibrium conditions, thus reproducing lateral exchange phenomena often recognized in structured media (Beven and Germann, 1982). Interdomain transfer processes are diffusion based and as such depend on the diffusivity of the matrix blocks and the geometric configuration of the preferred flow paths. When these processes are modeled by means of a first-order approximation (FOA), the system can be characterized by one unique parameter, the mass transfer rate coefficient. Despite extensive efforts in the past two decades, how closely the actual mass exchange process is captured by the first-order approximation and how to determine the transfer rate coefficients remain poorly understood.

First-order mass transfer models have been widely

used to interpret results from solute transport experiments. For certain conditions (e.g., negligible matrix domain flux, steady-state water flow and instantaneous adsorption), the transfer rate coefficients for solute (α_s) can be determined from moment analysis of the concentration breakthrough curve (BTC) (e.g., Valocchi, 1990). This methodology was tested by Hu and Brusseau (1995) in a series of leaching experiments through artificial soil columns. The authors explored different aggregate geometries, for which theoretical expressions of the transfer coefficients are available, and with most of the parameters of the two-region Mobile-Immobile Model (MIM) (van Genuchten and Wierenga, 1976) determined independently of the data.

In more general cases, for example when water moves through both the matrix and the macropore regions, experimental measurements of the mass exchange are difficult to make since more complex models with a large number of parameters are generally required. Matrix and macropore flows cannot be easily discriminated during water flow experiments, thus making the hydraulic characterization of the two domains very uncertain. On the basis of an analogy between water and solute transfer processes, Gerke and van Genuchten (1993b) suggested that the transfer rate coefficient for water (α_w) can be derived from the corresponding coefficient for solute (α_s), as determined using the MIM hypotheses. To date, this assumption has not been validated by experimental evidence, mostly because of technical limitations in monitoring the lateral exchange process.

We present results from infiltration experiments conducted on a soil column with an artificial macropore. Detailed knowledge of the geometry of the system and soil matrix properties, as well as the controlled laboratory conditions, allowed us to address some of the uncertainties mentioned above. For instance, we were able to discriminate matrix flow from macropore flow, and to measure the depth-integrated water exchange flux between the two domains. The experimental results were described reasonably well with a dual-permeability model, with most of the parameters determined independently of the data. A numerical analysis of the water transfer process also allowed us to determine the transfer rate coefficient for water, which otherwise would be a fitting parameter.

THEORY

The dual-permeability model (DPM) used in this study to simulate vertical water flow through a single-macropore column was described in detail by Gerke

P. Castiglione, B.P. Mohanty, P.J. Shouse, J. Simunek, M.Th. van Genuchten, George E. Brown, Jr. Salinity Laboratory, 450 W. Big Springs Road, USDA, ARS, Riverside, CA; and A. Santini, Department of Agricultural Engineering, University of Naples "Federico II", Italy. B.P. Mohanty, currently, Biological and Agricultural Engineering, Texas A&M University, College Station, TX. Received 14 June 2002. Original Research Paper. *Corresponding author (paoloc@uidaho.edu).

Abbreviations: BTC, breakthrough curve; DPM, dual-permeability model; FOA, first-order approximation; MIM, mobile-immobile model; PAM, polyacrylamide.

and van Genuchten (1993a). The governing equations for one-dimensional flow are

$$\frac{\partial \theta_f}{\partial t} = \frac{\partial}{\partial z} \left(K_f \frac{\partial h_f}{\partial z} - K_f \right) - \frac{\Gamma_w}{w_f} \quad [1]$$

$$\frac{\partial \theta_m}{\partial t} = \frac{\partial}{\partial z} \left(K_m \frac{\partial h_m}{\partial z} - K_m \right) + \frac{\Gamma_w}{1 - w_f} \quad [2]$$

in which the subscript “f” refers to the macropore domain, and “m” to the matrix domain; h (L) is the matric potential, K ($L T^{-1}$) the hydraulic conductivity, z (L) is the spatial coordinate, t (T) is time, Γ_w (T^{-1}) is the water transfer term, representing the flux of water being exchanged between macropores and the soil matrix per unit volume of bulk soil, and w_f is a dimensionless weighting factor. The volumetric water content θ_f in Eq. [1] is defined as the ratio of the volume of water of the fracture domain ($V_{w,f}$) to the total volume of fractures ($V_{t,f}$) $\theta_f = V_{w,f}/V_{t,f}$. Analogously, $\theta_m = V_{w,m}/V_{t,m}$. The volumetric weighting factor (w_f) is defined as the ratio of the fracture domain volume relative to the total soil volume (V_t):

$$w_f = V_{t,f}/V_t \quad [3]$$

While some macroscopic quantities, such as water content or flux, for a dual-permeability medium are defined as weighted averages of the corresponding properties of the individual domains, this cannot be done for the hydraulic conductivity, since in general no unique pressure head gradient exists (Beven and Germann, 1982). When the system is in hydraulic equilibrium ($h_f = h_m$), however, it is possible to define the hydraulic conductivity as (Peters and Klavetter, 1988):

$$K = w_f K_f + (1 - w_f) K_m \quad [4]$$

Equation [4] holds in particular for saturated conditions and thus permits us to estimate the macropore saturated conductivity ($K_{f,sat}$) from K_{sat} , $K_{m,sat}$, and w_f .

The interdomain water exchange flux is modeled by means of the first-order approximation (FOA):

$$\Gamma_w = \alpha_w (h_f - h_m) \quad [5]$$

in which h_f and h_m are averaged over some representative elementary volume, and α_w ($L^{-1} T^{-1}$) is the mass transfer rate coefficient for water. Assuming analogy between water and solute lateral exchange processes, Gerke and van Genuchten, (1993b) derived α_w from the equivalent transfer rate coefficient for solute. The FOA for solute exchange flux (Γ_s) is expressed as:

$$\Gamma_s = \alpha_s (c_f - c_m) \quad [6]$$

where α_s (T^{-1}) is the transfer rate coefficient for solute, and c_f and c_m ($M L^{-3}$) are the solute concentrations for the fracture and the matrix domain, respectively. Assuming applicability of MIM (van Genuchten and Wierenga, 1976), α_s is fully determined by geometry and diffusivity of the soil aggregates, and is generally approximated by the expression (van Genuchten and Dalton, 1986):

$$\alpha_s = \frac{H}{\lambda^2} \theta_m D_{a,m} \quad [7]$$

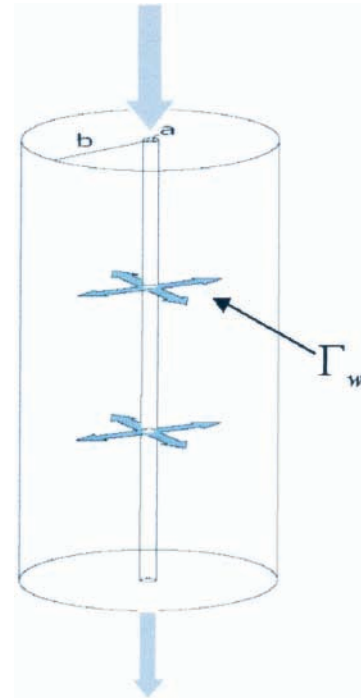


Fig. 1. Scheme of the soil column with a vertical cylindrical macropore.

where H is a dimensionless geometry-dependent coefficient and λ (L) is the characteristic length of the matrix structure (e.g., the radius for spherical or cylindrical aggregates, or one-half of the fracture spacing for parallel rectangular matrix blocks); $D_{a,m}$ ($L^2 T^{-1}$) is the effective diffusion coefficient of solute in the soil matrix (notice that the subscript “m” represents here the soil “matrix,” not the “mobile” domain as is commonly done in literature). For simple geometries of the aggregates, theoretical values for the geometrical parameters in Eq. [7] can be derived (Valocchi, 1990; van Genuchten and Dalton, 1986). In particular, several expressions are reported in literature for cylindrical macropores (van Genuchten and Dalton, 1986; Gerke and van Genuchten, 1996; Young and Ball, 1995), which we found to give very similar results. Below we adopt the expression proposed by Young and Ball (1995) to be used in Eq. [7]:

$$\lambda = b - a \quad [8]$$

$$H = \frac{8(\xi_0^2 - 1)(\xi_0 - 1)^2}{4\xi_0^4 \ln \xi_0 - 3\xi_0^4 + 4\xi_0^2 - 1}, \quad \text{with } \xi_0 = \frac{b}{a} \quad [9]$$

In Eq. [8] and [9], a is the radius of the macropore, and b is the radius of the soil mantle surrounding the macropore (see Fig. 1).

Due to their common diffusive nature, lateral water and solute transfers are often considered similar process (Dykhuizen, 1990; Gerke and van Genuchten, 1993a; Zimmerman et al., 1990). Assuming that the water flux divergence is zero within the soil matrix, Gerke and van Genuchten (1993b) found that the geometry of the aggregates affects water and solute mass transfers in the same way. They therefore proposed the following expression for the transfer rate coefficient for water:

$$\alpha_w = \frac{H}{\lambda^2} K_a \gamma_w \quad [10]$$

which is derived from Eq. [7] with the term $K_a \gamma_w$ replacing $\theta_m D_{a,m}$. In Eq. [10], γ_w is a dimensionless scaling factor and K_a ($L T^{-1}$) the effective hydraulic conductivity function of the macropore–matrix interface, evaluated in terms of both h_m and h_f as follows:

$$K_a = 0.5[K_a(h_m) + K_a(h_f)] \quad [11]$$

In the absence of organic matter or other deposits along the macropore wall (which may alter the permeability of the aggregates at the interface), K_a is best represented by the matrix conductivity function K_m (Gerke and van Genuchten, 1993a).

Gerke and van Genuchten (1993b) and Gerke and van Genuchten (1996) tested the applicability of Eq. [10] for several aggregate geometries (spherical, rectangular slab, and cylindrical macropores) by comparing simulation results of the one-dimensional DPM with those generated using equivalent two-dimensional geometry-based transport models. For simplicity, the effects of gravity were neglected in their calculations. These numerical studies revealed that, in general, Eq. [10] performs well as long as the dimensions of the matrix blocks are not too large. Their results also suggest that, provided Eq. [11] is used, an average value of 0.4 for the scaling factor γ_w should be reasonably applicable to all of the geometries investigated. This value, however, may not be appropriate for describing water exchange when the vertical water flow in the matrix is considered, or for initial and boundary conditions different from those used in the original studies of Gerke and van Genuchten (1993b). To take this scenario-related dependency into account, we performed a numerical analysis of the water exchange process in a single macropore system for the same initial and boundary conditions reproduced in our experiments. Our calculations allowed us to determine an optimal value for the scaling factor γ_w , which subsequently will be used in the analysis of our experimental data.

Numerical Analysis of the Water Transfer Process

We generated series of synthetic data for lateral water exchange by simulating water infiltration through a soil column with a single macropore, as depicted in Fig. 1. Since the process is axial-symmetric, a modified version of the two-dimensional HYDRUS-2D code (Simunek et al., 1999) could be used. The synthetic water transfer data were subsequently compared with results of the one-dimensional dual-permeability model to test the applicability of Eq. [8], and to determine a value of the scaling factor γ_w that best describes the exchange process for the initial and boundary conditions used in our experiments. For both the two- and the one-dimensional simulations, and for both the matrix and macropore domain, the initial pressure head profile varied linearly from -155 cm at the top to -135 cm at the bottom. The pressure head was equal to zero at the top of the column, while seepage conditions were imposed at the bottom bound-

ary. In our simulation we explicitly considered vertical water flow in the soil matrix.

Two-Dimensional Simulations

The HYDRUS-2D code solves the axial-symmetric flow equations in the r - z plane using a mass lumped Galerkin finite element scheme. The flow domain consisted of two connecting porous media: a single macropore ($r \leq 0.5$ mm) at the center and the surrounding matrix region. A very fine finite element grid, as well as small time steps (Δt_{\min} was 10^{-9} h), were used to increase the accuracy of the calculations. We initially experienced some numerical problems, even with a very fine discretization near the macropore–matrix interface. This was caused by the fact that in HYDRUS-2D the independent variables and hydraulic properties are assigned to nodes, and smoothed linearly between neighboring nodes, as is traditionally done in finite element schemes. This approach causes flow and transport properties to be smoothed across the interfaces between different materials. Most of the numerical problems were solved by modifying the code to allow assignment of material properties to elements, rather than to individual nodes.

The van Genuchten–Mualem model (van Genuchten, 1980) was used to describe the retention and conductivity functions of both the matrix and the macropore domain:

$$h(S_e) = \frac{1}{\alpha} \left[1 - (S_e^{-1/m} - 1)^{1/n} \right] \quad [12]$$

$$K(S_e) = K_s S_e^l \left[1 - (1 - S_e^{1/m})^m \right]^2 \quad [13]$$

where $Se = (\theta - \theta_r)/(\theta_s - \theta_r)$ is the effective saturation, α (L^{-1}), n and l are empirical parameters, θ_r is the residual water content, θ_s is the saturated water content, and K_s ($L T^{-1}$) is the saturated hydraulic conductivity. We used the $m = 1 - 1/n$ constraint so that each domain is characterized by a total of six parameters (hereafter referred to as “VGM parameters”). For our calculations, the matrix domain was assigned the VGM parameters estimated (as will be shown later) through inverse analysis of data from an infiltration experiment without a macropore ($\theta_s = 0.38$; $K_s = 0.08$ cm h^{-1} ; $l = 0.5$; $\theta_r = 0.20$, $\alpha = 0.005$, and $n = 1.664$). In contrast, three different hydraulic functions were considered for the macropore domain. The saturated conductivity ($K_{f,sat}$) was chosen equal to 2000, 20 000, and 100 000 cm h^{-1} , while the remaining parameters were in all cases fixed at $\theta_r = 0$, $\theta_s = 0.5$, $\alpha = 0.1$, $n = 2$, and $l = 0.5$. Two somewhat conflicting requirements were considered when choosing the VGM parameters for the macropore domain: (i) having a small air-entry tension (high α value), below which the hydraulic conductivity drops sharply to negligible values (high n value), and (ii) facilitating a stable numerical solution of the flow equations. Each simulation was repeated for three different soil mantle radii: 1.7, 2.7, and 12 cm.

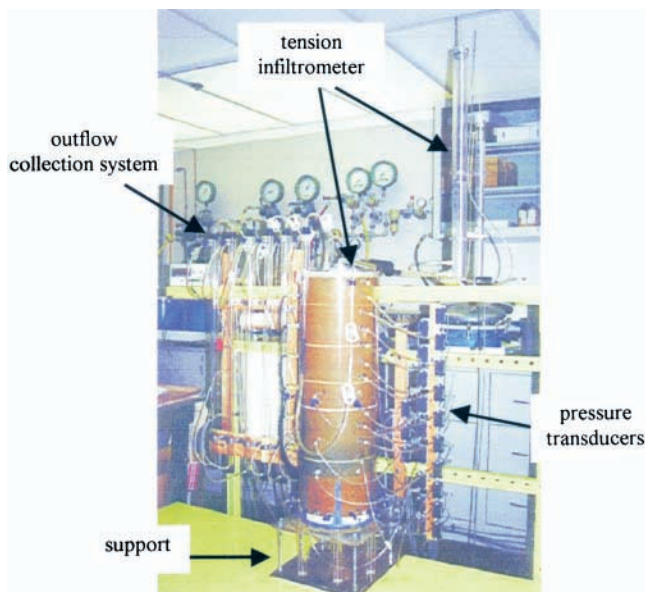


Fig. 2. Experimental setup.

One-Dimensional Simulations

Infiltration processes were simulated for the same scenarios (geometry, hydraulic properties, initial and boundary conditions) considered in the previous section using the one-dimensional DPM (as incorporated into HYDRUS-1D; Simunek et al., 1998). We next performed one-dimensional inverse analyses of the synthetic data to optimize γ_w , using cumulative mass transfer data in the objective function. Since optimized values for the transfer coefficient depend somewhat on the characteristic time scale of the synthetic data (Young and Ball, 1995), we homogenized the different series by extending each set of data to well after equilibrium was reached.

MATERIALS AND METHODS

Experimental Setup

A sandy loam (Typic Haploxeralf) with a small clay fraction (6%, mostly kaolinite) was used in this study because of its low shrink-swell capacity. The soil, collected from the Angeles National Forest (California) at 20 to 40 cm depth, was air-dried, sieved (2 mm), and packed into a large column in 3-cm increments to a dry bulk density of 1.56 g cm^{-3} . The column (Fig. 2) was made from an acrylic cylinder (75 cm deep; i.d. = 24 cm), resting on a specifically designed support for controlling the bottom boundary condition and collecting the drainage effluent (Fig. 3). The lower portion of the column was partitioned into six pie-shaped chambers using vertical dividers (Fig. 3). The dividers were made of 15-cm-high stainless-steel sheets, glued into grooves in the base plate and held rigidly by means of a vertical support placed in the center of the base plate. The base plate, also made of acrylic, housed six ceramic plates (bubbling pressure = $5 \times 10^4 \text{ Pa}$), one in each of the six chambers (Fig. 3). The ceramic plates were sealed into place with a system of rubber gaskets and removable cover panels. Drainage effluent from each chamber was collected separately in a system of six acrylic tubes (Fig. 2) that permitted automated measurement of the cumulative outflow using pressure transducers. The pressure head at the bottom of the soil column was regulated by adjusting the air pressure

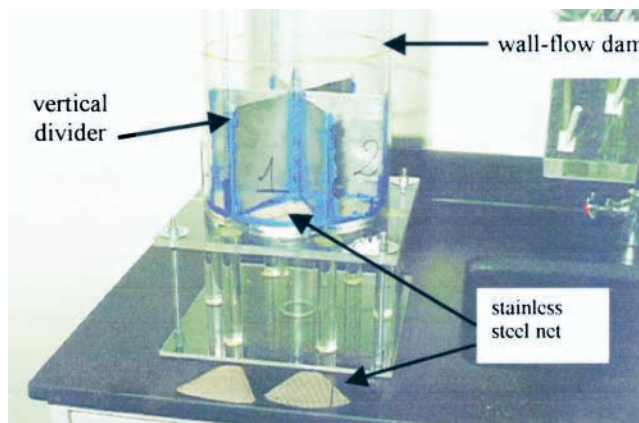


Fig. 3. Partitioning of the bottom of the column in six pie sectors. The metal dividers are 15 cm high. The stainless-steel nets support the soil when the ceramics are removed.

within the outflow tubes. A 3-cm layer of diatomaceous earth material (having a negligible hydraulic resistance) was placed in each chamber between the soil and the ceramic plates.

Collecting drainage effluent from each chamber independently allowed us to detect horizontal heterogeneities in the wetting front. In particular, we were able to verify the stability of the matrix flux in the absence of macropores. Most importantly, when a single artificial macropore was made and connected to one outflow chamber, separate measurements of the matrix and macropore fluxes could be obtained by contrasting the effluent fluxes from the different chambers. This methodology is applicable assuming preferential flow is fully confined within the artificial macropore. We prevented preferential flow along the column walls by inserting small glue rings (“wall flow dams”; see Fig. 3) at several depths on the internal wall of the column. The rings acted like a series of dams forcing any wall flow to reenter the soil matrix. Soil water pressure heads were measured using pencil-size tensiometers placed at 5-cm depth increments, while horizontal heterogeneities in the soil water pressure head were monitored using two sets of six tensiometers placed around the circumference of the soil column at depths of 50 and 75 cm below the soil surface. We also installed six time domain reflectometry three-rod probes (10 cm long) at 10-cm depth increments to measure the matrix water content profile.

Artificial Macropores

Different techniques for creating artificial macropores are described in the literature, depending on the objectives of the research, soil type, and column dimensions (Hu and Brusseau 1995; Li and Ghodrati, 1997; Czapar et al., 1992). In our study we created a single macropore by inserting a hollow stainless-steel tube (1-mm o.d.) from the surface into the soil matrix. The macropore was located approximately at the center of the column and reached the diatomaceous earth layer at the bottom of one of the chambers.

To help stabilize the artificial macropore, we applied a water-soluble polymer (polyacrylamide, PAM) along the macropore walls. This was done by pouring a PAM solution (75 g L^{-1}) into the stainless-steel tube once it was fully inserted into the soil. The tube was subsequently slowly removed from the soil such that the PAM left a coating on the macropore walls. To enhance diffusion into the surrounding matrix, the PAM was applied when the column was dry. After application, the column was left for 48 h before a new experiment was performed. While the technique proved effective, the macropore

itself was not always perfectly stable, and new applications of the polymer were needed periodically between separate flow experiments.

Experimental Procedure

Using a 0.33 g L^{-1} CaCl_2 solution, several infiltration and drainage experiments were performed before making the artificial macropore. These initial experiments were used to test the functionality of the experimental setup, especially the active drainage system, and to verify the uniformity of water flow through the soil column. A first-type boundary condition was imposed at the soil surface during the infiltration experiments by means of a tension infiltrometer (Ankeny et al., 1988; Perroux and White, 1988); this also permitted us to measure the infiltration rate. We used a disk (Soil Measurement Systems, Tucson, AZ) with the same diameter as the column, so that flow was always one-dimensional. A thin sand layer was placed on the soil surface to ensure perfect contact between soil and the infiltrometer. The head loss through the sand was measured by means of a very small tensiometer placed at the sand–soil interface.

One major challenge of the experimental setup was accurate control of the bottom boundary condition. When a tension is imposed through the ceramic plates, the presence of entrapped air, as well as the existence of fluxes greater than the conductivity of the ceramic plates, may cause the effective bottom tension to diverge from the applied one. Such a situation could lead to misinterpretations of the experimental results, particularly since the magnitude of the flux through the artificial macropore is not known a priori. We therefore designed the base of the column to allow us to remove or install different ceramic plates as needed. For example, to facilitate drainage from the column we applied tension at the bottom, whereas the ceramics were removed during the infiltration experiments to produce a seepage-type bottom boundary condition.

We present results for two infiltration experiments, one with and one without the artificial macropore, performed under identical initial and boundary conditions. The effects of the macropore on the overall flow regime were deduced by contrasting the measured inflow and outflow rates. In both experiments, the column was initially drained by applying suction at the bottom ($h = -250 \text{ cm}$). Pressure head profiles during the drainage showed fairly uniform values in the upper three-quarters of the column, and a steep decrease in the pressure head in the lower portion. Once a nearly uniformly dry profile was obtained in the upper three-quarters of the column, the ceramic plates were removed and the column was left to equilibrate for about 1 wk. Having a relatively low initial water content distribution favored extensive lateral exchange of water during the macropore infiltration experiment. In both experiments, the top pressure head equaled zero, while a seepage boundary condition was applied at the bottom by removing the ceramic plates.

RESULTS AND DISCUSSION

Results from Numerical Simulations

Results from the two-dimensional simulations highlighted several factors affecting the water exchange between the macropore and matrix. In general, water flow in the two regions did not evolve independently (i.e., based on their specific hydraulic properties), but were very much affected by each other. For example, the wetting front in the macropore had a tendency to slow down because of diffusion of water into the surrounding

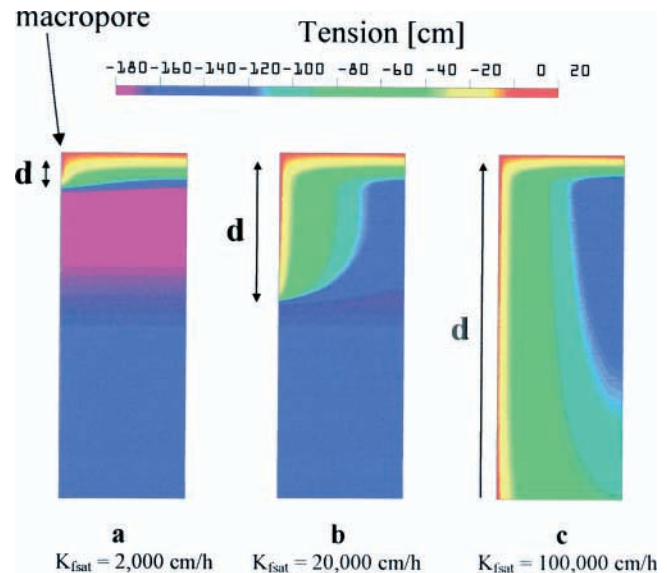


Fig. 4. Two dimensional simulations of pressure head distribution during infiltration processes for a 2.7-cm soil mantle. All figures show snapshots at 0.05 h.

matrix. This lateral exchange process is evident in Fig. 4, which shows snapshots ($t = 0.05 \text{ h}$) of the infiltration process simulated for three values of $K_{f,\text{sat}}$. Notice that the relative position of the two wetting fronts determined the longitudinal extent of the region affected by transfer process (indicated with d in Fig. 4). Since this region is large for highly conductive macropores, the depth-integrated water exchange rate is higher for larger $K_{f,\text{sat}}$ values. This result is also evident from Fig. 5, where the cumulative transfer flux integrated over the entire column is shown for the different scenarios. For each radius of the soil mantle, the water exchange rate is higher for higher macropore conductivity. Notice also that the total amount of exchanged water depends only on the size of the soil mantle for the smallest radius (Fig. 5b), whereas for larger mantles it also depends on $K_{f,\text{sat}}$ (Fig. 5a). This is due to vertical flow of water entering the matrix region from the top. In general, the maximum value of the cumulative transfer rate is smaller when vertical flow in the matrix is relatively fast compared with that of the macropore (smaller $K_{f,\text{sat}}$), since the pressure difference between the two domains (i.e., the driving force for water exchange) will vanish sooner. This effect is negligible for the smallest radii, for which equilibrium is reached only in a relatively short time.

Comparing the results from two- and one-dimensional simulations, we found that when the scaling factor γ_w in Eq. [8] was set equal to 1, water transfer rates predicted with the dual-permeability model were higher than those calculated with the two-dimensional simulations, as shown in Fig. 6 for a 12-cm soil mantle and $K_{f,\text{sat}} = 100\,000 \text{ cm h}^{-1}$. These results are consistent with those obtained by Gerke and van Genuchten (1993b). When optimized values of the scaling factor were used, the DPM reproduced the synthetic data more closely, not only in terms of the cumulative water exchange (Fig. 6), but also for the inflow and outflow rates. The optimized scaling factors are listed in Table 1 for the

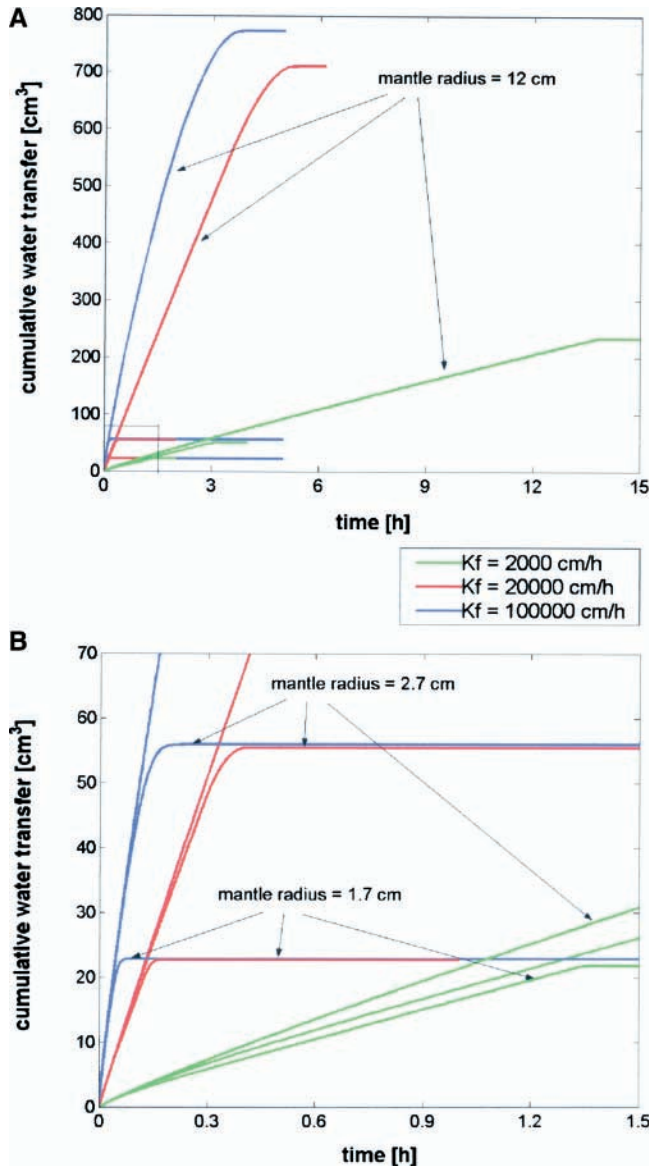


Fig. 5. Summary of the cumulative water transfer for nine two-dimensional simulations.

different scenarios considered. In particular, data for the 12-cm soil mantle radius (the radius of our experimental column) allowed us to determine an appropriate value for the transfer coefficient in subsequent analyses of the experimental results. The data are plotted in Fig. 7 against $K_{f,sat}$. The dependency of the scaling factor on the macropore saturated conductivity appears pronounced for the lowest $K_{f,sat}$, whereas γ_w approaches a fairly constant value for high $K_{f,sat}$ values. We note that Gerke and van Genuchten (1993b), who explored different hydraulic properties for the matrix domain in their numerical analysis, also found a slight variability of γ_w with the matrix hydraulic conductivity. Although our results cannot be directly compared with the findings of Gerke and van Genuchten (1993b) (since different boundary conditions were adopted in the two studies, and since we explicitly took into account the vertical water movement in the matrix domain), it appears that, in general,

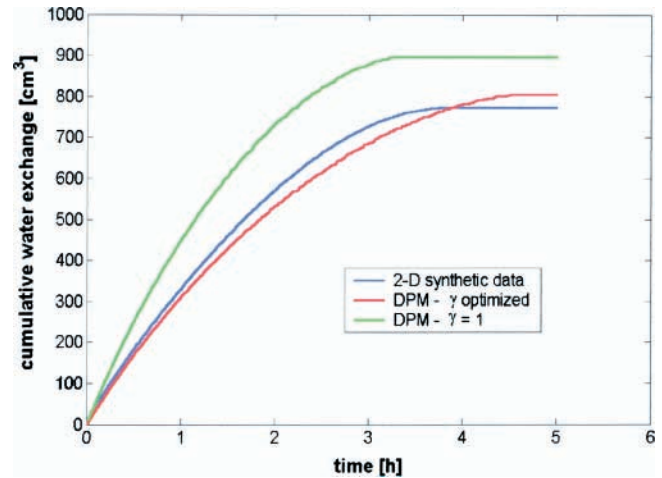


Fig. 6. Cumulative water exchange predicted by the one-dimensional dual-permeability model (DPM) compared with the transfer calculated by HYDRUS 2-D.

the scaling factor γ_w is correlated to the ratio of the two domain's conductivities.

Infiltration Experiment without Macropores

Water flow during infiltration without the macropore appeared to occur under equilibrium conditions. This was evident from visual inspection of the sharp wetting front and from the analysis of the data, which were well described using the Richards equation (see Fig. 8 and 9). The cumulative inflow curve displayed a pronounced sorption phase at the beginning of the infiltration (Fig. 8). During this stage, the infiltration rate was high, being driven by both capillary and gravity forces. As the wetting front moves down, pressure head gradients eventually become negligible and the infiltration rate approaches a constant value, roughly equal to the saturated hydraulic conductivity. Outflow started about 13 h later and rapidly became constant and equal to the inflow rate. The total effluent was evenly distributed among the six chambers (data not shown), and the column at this time appeared thoroughly saturated (Fig. 9).

Data from the infiltration experiment were used to characterize the soil matrix hydraulic properties. We used the HYDRUS-1D code (Simunek et al., 1998) for inverse analysis (e.g., Hopmans et al., 2002) using inflow, outflow, and tension data. Of the six VGM parameters, we measured θ_s independently of the infiltration experiment ($\theta_s = 0.38$), determined K_s from the steady-state

Table 1. Optimized values of the scaling factor γ_w for different soil mantle radii and macropore saturated hydraulic conductivities.

Mantle radius	$K_{f,sat}$	Optimized γ_w
cm	cm h ⁻¹	
1.7	2 000	0.0487
	20 000	0.1991
	100 000	0.6062
2.7	2 000	0.1008
	20 000	0.2402
	100 000	0.6874
12	2 000	0.1026
	8 000	0.2792
	20 000	0.4033
	100 000	0.6348

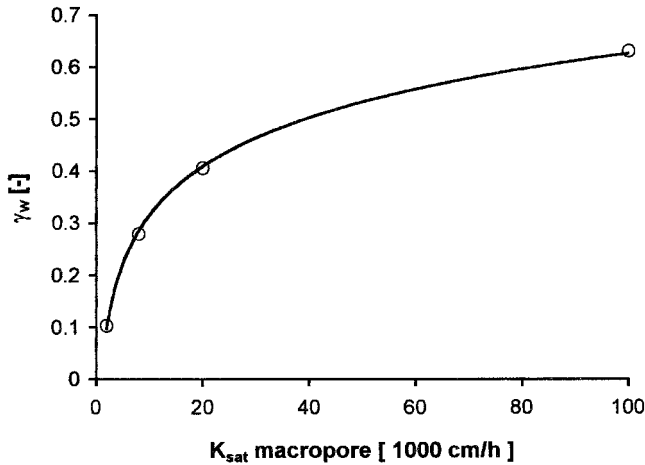


Fig. 7. Scaling factor dependency on the macropore saturated conductivity.

infiltration rate ($K_s = 0.08 \text{ cm h}^{-1}$), and fixed l to 0.5, whereas the remaining three parameters were optimized ($\theta_r = 0.20$, $\alpha = 0.005$, and $n = 1.664$). Good correspondence was obtained between the fitted and measured data (Fig. 8 and 9). The uniqueness of the solution was empirically verified by repeating the inverse analysis with different initial values of the unknown parameters. We note, however, that the estimated hydraulic properties probably were somewhat biased by a lack of information of soil matrix hydraulic behavior in the dry range (because of the dimension of the column, it was not possible to achieve very dry conditions). Nevertheless, the hydraulic characteristics in the wet range, which are of interest in this study, were successfully estimated from the available data. In particular, the early stage of the infiltration process should define the soil matrix diffusivity, which regulates interdomain exchange, and ultimately determines the strength of macropore flow.

Infiltration Experiment with One Artificial Macropore

From capillary theory, a top boundary pressure head greater than -3 cm was needed to initiate flow through

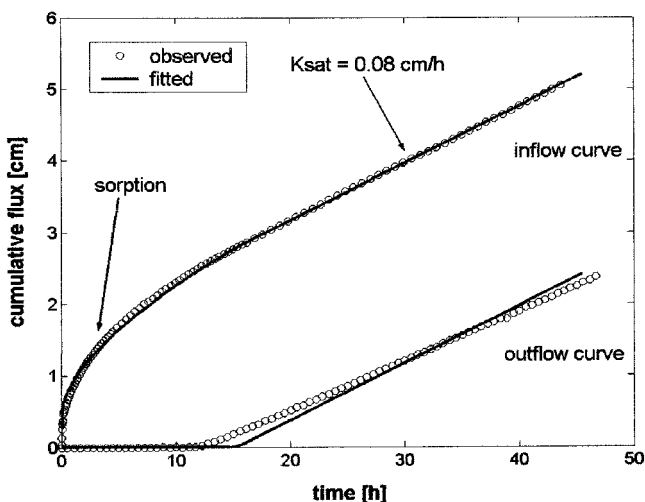


Fig. 8. Measured and fitted inflow and outflow curves during infiltration in the homogeneous soil column (without macropore). Simulated results are obtained using Richards' equation.

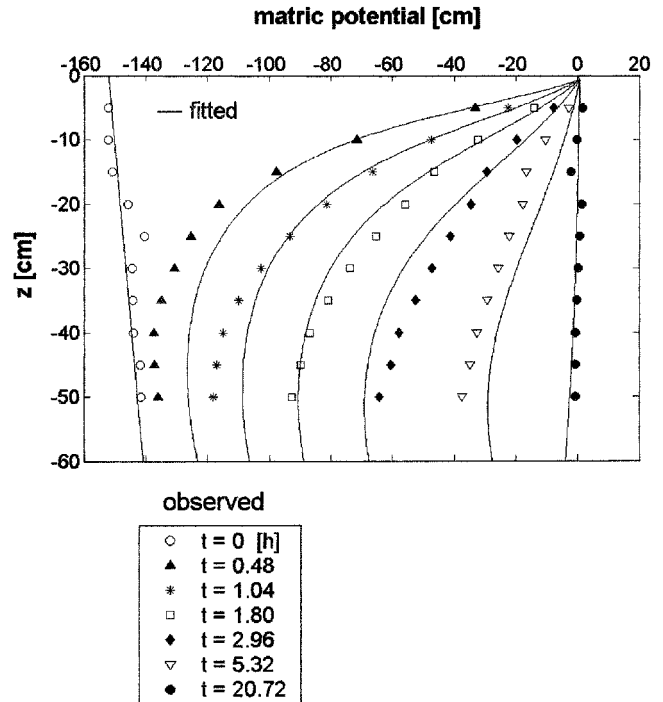


Fig. 9. Pressure head profiles during the infiltration experiments without the macropore. Simulated results are obtained using Richards' equation.

the 1-mm-diameter macropore. The occurrence of macropore flow was immediately evident, since the infiltration rate was considerably higher than that observed without the macropore (Fig. 10). Furthermore, after about 45 min a roughly constant flux was observed in the chamber where the macropore was located, while no outflow was observed in the other chambers (data not shown). This flux, 0.082 cm h^{-1} , was therefore assumed to be all macropore outflow (O_f). This experiment allowed us to discriminate between macropore flow and matrix flow, and to measure the interdomain exchange flux. We reproduced the same initial and boundary conditions as for the infiltration experiment without a macropore. In particular, a zero pressure head was maintained at the top. During infiltration, the fol-

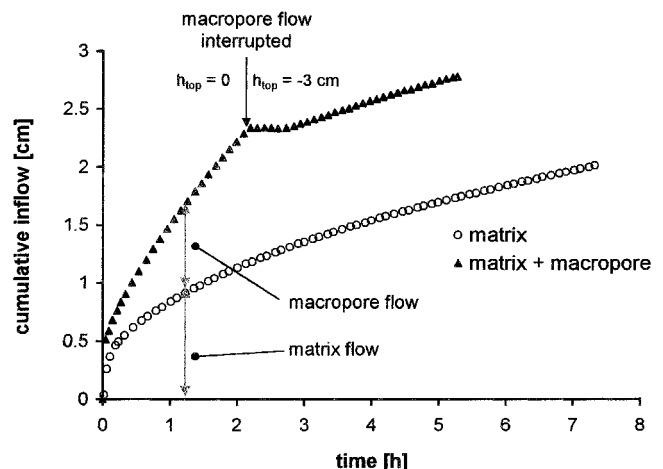


Fig. 10. Cumulative infiltration rates measured with and without the macropore.

lowing relationship holds:

$$I_{\text{tot}}(t) = I_m(t) + I_f(t) \quad [14]$$

where I_m is the flux of water infiltrating into the soil matrix, I_f is the flux entering the macropore, and I_{tot} represents the total infiltration rate, as measured with the tension infiltrometer. An analogous relationship can be written for the outlet flux:

$$O_{\text{tot}}(t) = O_m(t) + O_f(t) \quad [15]$$

where O_m and O_f are the contributions of matrix and macropore, respectively, to the total outflow (O_{tot}). Because of lateral diffusion, in general $I_f > O_f$, the difference between the two fluxes representing the total water flux exchanged between macropore and matrix:

$$\bar{\Gamma}_w(t) = I_f(t) - O_f(t) \quad [16]$$

Note the different symbols for the local (Γ_w) and the depth-integrated exchange flux ($\bar{\Gamma}_w$). The flux entering the macropore (I_f) could not be measured directly. Nonetheless, assuming that I_m in Eq. [14] equals the infiltration rate measured during the experiment without the macropore, and hence that the presence of the macropore does not affect the matrix flux, I_f could be estimated from the difference between the inflow rates observed during the two experiments (Fig. 10). This assumption seems very reasonable at the early stage of the process, when lateral diffusion is still confined to only a relatively small portion of the column. As the infiltration process proceeds, however, the assumption will become unrealistic, especially if lateral equilibration is relatively fast. The validity of the above assumption was tested by suddenly interrupting the macropore flow process (before steady-state conditions were reached) and verifying that the cumulative infiltration curve proceeded parallel to the corresponding nonmacropore curve (see Fig. 10). Macropore flow was interrupted by reducing the top pressure head to below the macropore air-entry-value (-3 cm). Several steady-state experiments without macropores had previously revealed that such a small pressure drop did not affect the matrix flow rate. Following the interruption, bubbling in the Mariotte and the reservoir towers of the tension infiltrometer stopped for several minutes until the new pressure head was established at the top boundary. During this period the instrument could not record the matrix water flow, which explains the short horizontal segment in the cumulative infiltration data shown in Fig. 10. The total exchange flux during the macropore infiltration process can therefore be measured as

$$\bar{\Gamma}_w = (I_{\text{tot}} - I_m) - O_f \quad [17]$$

The cumulative lateral flux measured in this way is shown in Fig. 11, and will be discussed in more detail below. The experiment was repeated three times, with the three replications giving nearly identical results (not shown here). We emphasize here that steady-state conditions could never be reached completely because of slow, yet persistent clogging of the macropore during infiltration.

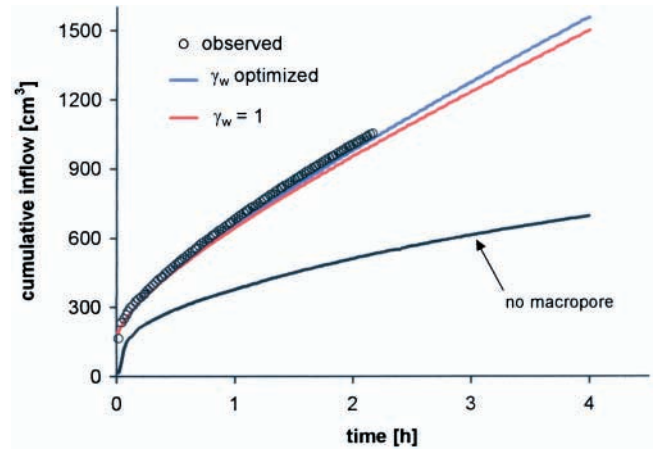


Fig. 11. Cumulative infiltration curves measured in the soil column with a macropore, and calculated using the dual permeability model, for γ_w optimized and $\gamma_w = 1$.

Comparisons of Model Results with Experimental Data

Application of the DPM involves two sets of VGM parameters, one for each domain, plus the mass transfer rate coefficient (α_w) and the volumetric weighting factor (w_f). In our case, w_f is known from the geometry of the system ($w_f = 1.8 \times 10^{-5}$). The characteristics of the matrix domain were determined from an analysis of the infiltration data without the macropore. Estimation of the macropore parameters was much more uncertain, even for the controlled conditions of our experiment. A single macropore remains either completely full or nearly empty, except possibly for some film flow, so that its behavior during variably saturated flow cannot be easily investigated. Still, this behavior suggests that the macropore conductivity function, $K_f(h_f)$, should be characterized by a sharp drop to negligible values after a very small air-entry suction is exceeded. This representation of a cylindrical macropore as an equivalent porous medium reduced the range of possible values for the macropore domain hydraulic parameters.

Since it was not possible to maintain macropore flow until steady-state conditions were reached, Eq. [4] could not be used to estimate the saturated hydraulic conductivity. We optimized $K_{f,\text{sat}}$ by fitting this parameter to the inflow data using the parameter estimation feature of HYDRUS-1D. Cumulative infiltration rates were found to be sensitive to $K_{f,\text{sat}}$, but not affected by the other hydraulic parameters. Our measured data were closely reproduced when using $K_{f,\text{sat}} = 25\,000$ cm h⁻¹ (Fig. 11). The contribution of the macropore to the composite soil saturated conductivity (K_{sat}) can now be estimated from Eq. [4]: for $K_{f,\text{sat}} = 25\,000$ cm h⁻¹ and $w_f = 1.8 \times 10^{-5}$, K_{sat} was found to be equal to 0.45 cm h⁻¹, as compared with a value of only 0.08 cm h⁻¹ as observed in the absence of the macropore. The scaling factor corresponding to this value was obtained from Fig. 7 ($\gamma_w = 0.441$). Three of the six VGM parameters for the macropore domain were fixed ($\theta_r = 0$, $\theta_s = 0.5$, $l = 0.5$), while the remaining parameters were determined by fitting lateral exchange and outflow data, on

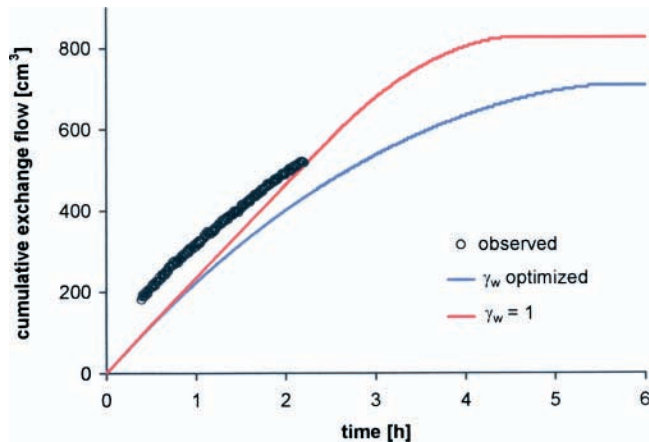


Fig. 12. Observed vs. predicted cumulative water transfer between the macropore and matrix. In the dual permeability model, both γ_w optimized and $\gamma_w = 1$ were used.

which they appear to have the largest impact. Least squares fitting gave $\alpha = 0.1 \text{ cm}^{-1}$; $n = 2$.

To highlight the model sensitivity to the scaling factor, we compared the experimental data with the model results obtained with both the optimized value of the γ_w parameter, and for $\gamma_w = 1$. In both cases, the cumulative water exchange predicted with the DPM did not match the experimental data perfectly (Fig. 12). However, the calculated water transfer rate (given by the slope of the cumulative curve) reproduced the observations reasonably well when using the optimized scaling factor, while it persistently overestimated the experimental results with $\gamma_w = 1$. Even with the optimized γ_w , an offset of about 80 cm^3 was still observed between the experimental and simulated cumulative curves. Assuming a porosity of 0.45 for the fine sand placed on top of the column, this amount corresponds to water adsorbed in about 0.4 cm of sand after infiltration started. Therefore, the disagreement between measured and calculated data in Fig. 12 may be attributed to a slight difference in the thickness of the sand layer between macropore and non-macropore experiments.

Finally, we show in Fig. 13 the impact of the scaling factor on cumulative outflow. The relative poor comparison with the experimental results indicates several limitations of the DPM model. For example, we observed a constant effluent flux until the preferential flow was interrupted, whereas the simulation predicted a progressively increasing outflow rate. This behavior resulted from having a constant flux at the inlet and progressively less exchange of water between the macropore and the matrix as equilibrium is approached. An excellent match was obtained between the experimental and simulated (with optimized γ_w) time intervals between the beginning of the infiltration process and the appearance of the first outflow. For $\gamma_w = 1$, the DPM failed to predict the breakthrough time.

CONCLUSIONS

Experiments in artificial macroporous systems provide insight into preferential flow phenomena that would be difficult to achieve otherwise. In this study

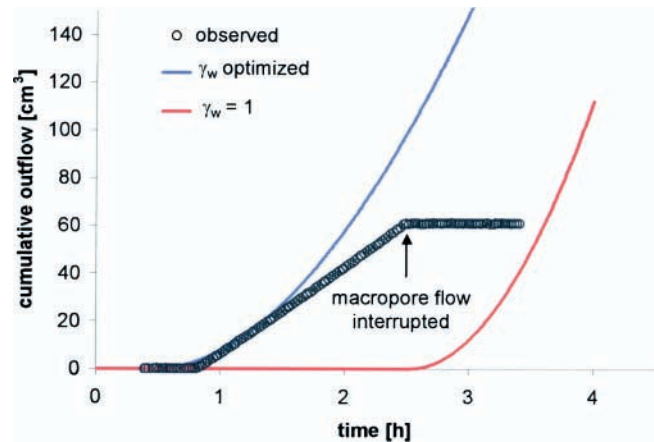


Fig. 13. Observed vs. predicted cumulative outflow. In the dual permeability model, both γ_w optimized and $\gamma_w = 1$ were used.

we discriminate macropore flow and matrix flow. In addition, the water exchange flux integrated over the column was measured. The experimental data were described reasonably well with the dual-permeability model, with most of the parameters determined independently of the observations. For the investigated geometry, the first-order approximation closely described the water transfer data as long as an appropriate value for the transfer rate coefficient (or equivalently for the correcting scaling factor γ_w) was used.

Similarly to the previous study by Gerke and van Genuchten (1993b), we derived the transfer rate coefficient for water from the equivalent coefficient for solute transfer through numerical simulations of the lateral diffusion process. Our analysis showed that the scaling factor γ_w , in general, is dependent on the hydraulic conductivity of the macropore domain.

ACKNOWLEDGMENTS

The research was conducted at the George E. Brown Jr. Salinity Laboratory, Riverside, CA. P. Castiglione would like to acknowledge the financial support from the University of Naples, Italy, during his stay at Riverside as part of his Ph.D. research. The authors also acknowledge the technical support of J. Fargerlund and J.A. Jobes. This study was partially supported by NSF grant EAR-0106956.

REFERENCES

- Ankeny, M.D., T.C. Kaspar, and A.A. Hussen. 1988. Designed for an automated tension infiltrometer. *Soil Sci. Soc. Am. J.* 52:893–895.
- Beven, K.J., and P. Germann. 1982. Macropores and water flow in soils. *Water Resour. Res.* 18:1311–1325.
- Cushman, J.H. 1990. An introduction to hierarchical porous media. p. 1–6. *In* J.H. Cushman (ed.) *Dynamics of fluids in hierarchical porous media*. Academic Press, London.
- Czapar, G.F., R. Horton, and R.S. Fawcett. 1992. Herbicide and tracer movement in soil columns containing an artificial macropore. *J. Environ. Qual.* 21:110–115.
- Dykhuizen, R.C. 1990. A new coupling term for dual-porosity models. *Water Resour. Res.* 26:351–356.
- Gerke, H.H., and M.Th. van Genuchten. 1993a. A dual-porosity model for simulating the preferential movement of water and solutes in structured porous media. *Water Resour. Res.* 29:305–319.
- Gerke, H.H., and M.Th. van Genuchten. 1993b. Evaluation of a 1st-order water transfer term for variably saturated dual-porosity flow models. *Water Resour. Res.* 29:1225–1238.

- Gerke, H.H., and M.Th. van Genuchten. 1996. Macroscopic representation of structural geometry for simulating water and solute movement in dual-porosity media. *Adv. Water Resour.* 19:343–357.
- Hopmans, J.W., J. Simunek, N. Romano, and W. Durner. 2002. Inverse modeling of transient water flow. p. 963–1008. *In* J.H. Dane and G.C. Topp (ed.) *Methods of soil analysis. Part 4. SSSA Book Ser. 5.* SSSA, Madison, WI.
- Hu, Q.H., and M.L. Brusseau. 1995. Effect of solute size on transport in structured porous media. *Water Resour. Res.* 31:1637–1646.
- Li, Y.M., and M. Ghodrati. 1997. Preferential transport of solute through soil columns containing constructed macropores. *Soil Sci. Soc. Am. J.* 61:1308–1317.
- National Research Council. 2001. *Conceptual models of flow and transport in the fractured vadose zone.* National Academy Press, Washington, DC.
- Othmer, H., B. Diekkruger, and M. Kutilek. 1991. Bimodal porosity and unsaturated hydraulic conductivity. *Soil Sci.* 152:139–150.
- Perroux, K.M., and I. White. 1988. Designs for disc permeameters. *Soil Sci. Soc. Am. J.* 52:1205–1214.
- Peters, R.R., and E.A. Klavetter. 1988. A continuum model for water movement in an unsaturated fractured rock mass. *Water Resour. Res.* 24:416–430.
- Pruess, K. 1999. A mechanistic model for water seepage through thick unsaturated zones in fractured rocks of low matrix permeability. *Water Resour. Res.* 34:1039–1051.
- Simunek, J., M. Sejna, and M.Th. van Genuchten. 1998. The HYDRUS-1D software package for simulating the one-dimensional movement of water, heat, and multiple solutes in variably-saturated media. Version 2.0. IGWMC-TPS-70. International Ground Water Modeling Center, Colorado School of Mines, Golden, CO.
- Simunek, J., M. Sejna, and M.Th. van Genuchten. 1999. The HYDRUS-2D software package for simulating two-dimensional movement of water, heat, and multiple solutes in variably saturated media. Version 2.0. IGWMC-TPS-53. International Ground Water Modeling Center, Colorado School of Mines, Golden, CO.
- Smettem, K.R.J., and C. Kirkby. 1990. Measuring the hydraulic properties of a stable aggregated soil. *J. Hydrol. (Amsterdam)* 117:1–13.
- Valocchi, A.J. 1990. Use of temporal moment analysis to study reactive solute transport in aggregated porous media. *Geoderma* 46: 233–247.
- van Genuchten, M.Th., and P.J. Wierenga. 1976. Mass transfer studies in sorbing porous media. I. Analytical solutions. *Soil Sci. Soc. Am. J.* 40:473–480.
- van Genuchten, M.Th. 1980. A closed-form equation for predicting the hydraulic conductivity of unsaturated soils. *Soil Sci. Soc. Am. J.* 44:892–898.
- van Genuchten, M.Th., and F.N. Dalton. 1986. Models for simulating salt movement in aggregated field soils. *Geoderma* 38:165–183.
- Young, D.F., and W.P. Ball. 1995. Effects of column conditions on the first-order rate modeling of non-equilibrium solute breakthrough. *Water Resour. Res.* 31:2181–2192.
- Zimmerman, R.W., G.S. Bodvarsson, and E.M. Kwicklis. 1990. Absorption of water into porous blocks of various shapes and sizes. *Water Resour. Res.* 26:2797–2806.